Setting Boundary Conditions For Slotted Throat Wind Tunnels Using Calorically Imperfect Gas Assumptions

J.-R. Carlson*

NASA Langley Research Center, Hampton, VA 23681

The derivation and application of two back pressure controlling methods for setting the dynamic pressure, Mach number, and Reynolds number of subsonic wind tunnels with a slotted-throat test section are discussed. The first method uses a pressure difference to determine the tunnel dynamic pressure via the compressible Bernoulli equations and is used in the ideal gas path in the CFD code. The second method uses an enthalpy difference in the flow to determine the velocity in the test section and can be applied to multispecies, calorically imperfect and calorically perfect gas flow simulations. For a tunnel operating point close to standard atmosphere conditions, Mach number, pressure, and temperature along the tunnel centerline were very closely matched between the various thermodynamic equation assumption controller methods.

I. Nomenclature

A	area, m^2
c_p	specific heat at constant pressure, J/kg-K
c_v	specific heat at constant volume, J/kg-K
c	speed of sound, m/s
C_p	pressure coefficient
H	enthalpy, J/kg
$\mathcal{K}$	calibration constant
K_1	pressure loss coefficient
M	Mach number
p	pressure, Pa
q	dynamic pressure, Pa
r	radius, m
Re	unit Reynolds number, 1/m
T	temperature, K
V	velocity, m/s
x,y	Cartesian directions
R_s	specific gas constant, J/kg-K
R_m	universal gas constant, 287.053 J/kg-K

Subscripts

back	back pressure
CL	centerline
inflow	at location of inflow boundary
BM	bell mouth
ref	reference conditions
SC	settling chamber

*Research Scientist, Computational AeroSciences Branch, Mail Stop 128, Associate Fellow AIAA.

t	total conditions
TS	test section
exit	at location of exit boundary
∞	freestream condition

Conventions

CFD	computational fluid dynamics
PBC	static pressure outflow boundary condition
PTBC	total pressure inflow boundary condition
Sta.	tunnel station, m
TTBC	total temperature inflow boundary condition

Symbols

γ	ratio of specific heats, (1.4 for air)
μ	bulk viscosity, kg/m-sec
ρ	density, kg/m^3
$\tilde{}$	dimensional quantity

II. Introduction

Ongoing efforts have been underway to develop and improve computational fluid dynamic (CFD) modeling of the flow in NASA Langley Research Center tunnels such as the Transonic Dynamics Tunnel (TDT) and the National Transonic Facility (NTF). There continue to be questions concerning the best physical configuration to use downstream of the test section (e.g. diffuser length truncation, diffuser extensions, or alternate geometry diffuser models), as well as how to best define the outflow boundary condition, all to achieve a useful facsimile of the actual flow in the tunnel test section. Concerning the later point, a tunnel back-pressure controller [1] was developed during the Junction Flow experiments [2, 3] performed in the Langley 14- by 22-Foot Subsonic Tunnel. The controller monitors pressures in the tunnel circuit, processes the data using a set of tunnel operating equations and passes the results to a Proportional-Integral-Derivative (PID) controller method to adjust the level of the back pressure boundary condition. This paper advances the previous back pressure controller method to modeling tunnels with a slotted-throat test section and extends the gas thermodynamic assumptions of the controller to include thermally imperfect and thermally perfect thermodynamic equations of state, as well as account for multispecies mixtures in the tunnel flow medium.

III. Survey of Subsonic Tunnel Operating Equations

In order to make an acceptably accurate statement about the condition of the flow in the test section, the thermodynamic state of the tunnel must be measured in a sufficiently unbiased fashion to arrive at the same flow conditions regardless of the contents of the test section, i.e., with or without a test article installed. Calibration and condition setting equations can vary depending on the tunnel design, and flow speed, pressure, temperature, and medium. Subsonic, atmospheric tunnels like the NASA Langley 14- by 22-Foot Subsonic Tunnel (14x22), when run in the closed throat configuration, can have different measurement and data analysis systems compared to pressurized, heavy gas tunnels with a slotted test section, such as the NASA Langley Transonic Dynamics Tunnel (TDT).

The following sections review the background of the incompressible calibration equations that are typical of subsonic closed-throat wind tunnels, followed by a discussion of equations applicable to compressible air using ideal gas and more general gas mixtures for both thermally imperfect and perfect gas models.

A. Incompressible Bernoulli Method

This method determines the speed of a subsonic wind tunnel using the incompressible Bernoulli's equation, Eq. 1, together with the continuity equation, Eq. 2. Pressure data from two points upstream the tunnel test section are used to calculate the dynamic pressure in the test section. Further discussion on this theory can be found in Pope [4]. A

sketch of the measurement locations are shown in Fig. 1.

$$p_L + q_L = p_S + q_S - K_1 q_S \tag{1}$$

$$(VA)\big|_L = (VA)\big|_S \tag{2}$$

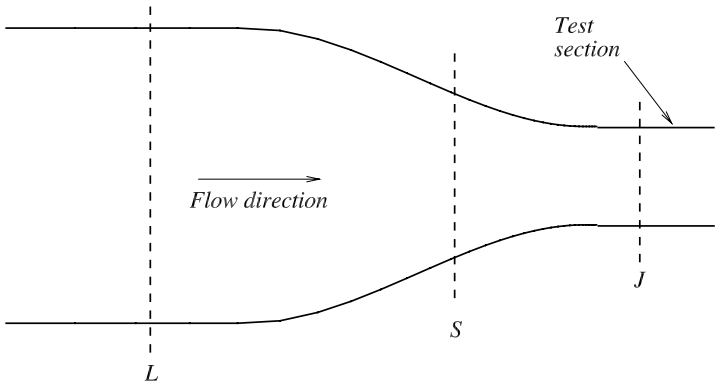

Figure 1. Schematic of the two-point method, (Ref. [4], Fig. 3.29).

The first point, at *L*, measures the pressure of the tunnel flow in the large settling chamber and the second point, at *S*, measures the pressure just upstream of the test section. The expectation, and primary assumption, is that the flow measurement at *S* is not significantly influenced by the presence of a model in the test section at *J*.[a] The density terms in the continuity equation are constants due to the incompressible flow assumption and so drop out in these equations. The continuity equation, Eq. 2, is used to derive expressions for the dynamic pressures q_L and q_S.

$$q_L = q_S \left(\frac{A_S}{A_L}\right)^2, \quad q_S = q_J \left(\frac{A_J}{A_S}\right)^2 \tag{3}$$

Substituting Eq. 3 into Eq. 1 and reducing $\left[1 - K_1 - \left(\frac{A_S}{A_L}\right)^2\right]\left(\frac{A_J}{A_S}\right)^2$ to a single constant, $\mathcal{K}$, creates an expression relating the upstream pressure difference to the dynamic pressure in the tunnel test section, Eq. 4.

$$p_L - p_S = \mathcal{K}\, q_J \tag{4}$$

If the settling chamber Mach number is very low, then the pressure ratio in that location is very close to unity, Eq. 5. For $M_L < 0.05$, the local static pressure is within 0.2% of the local total pressure. With the substitution of the total pressure into Eq. 4, the calibration equation is written as Eq.6.

$$0.9983 \lessapprox \left(1 + \frac{\gamma - 1}{2} M_L^2\right)^{-\gamma/\gamma - 1} < 1.0, \text{ so that } p_L \approx p_{t,L} \tag{5}$$

$$p_{t,L} - p_S = \mathcal{K}\, q_J \tag{6}$$

Using the theory just outlined, the dynamic pressure, equivalent freestream static pressure, and tunnel Mach number in a wind tunnel can be calculated. The following nomenclature is adopted: SC = settling chamber, BM = bell mouth, and TS = test section for L, S, and J, respectively, as defined in the previous section. Equation 7 is then the form of the equation for operating the tunnel. Several procedures exist for determining the values of the calibration parameter, $\mathcal{K}$.

$$q_{\mathrm{BM,incompressible}} = p_{t,\mathrm{SC}} - p_{\mathrm{BM}} \tag{7}$$

For this discussion, a single point calibration will be used to demonstrate the process. Notional locations for these survey stations are shown in Fig. 2. A probe is placed along the centerline of the test section to measure the total

[a] Each facility and calibration process could guide the choice of *S* and decide what may constitute a significant degree of influence.

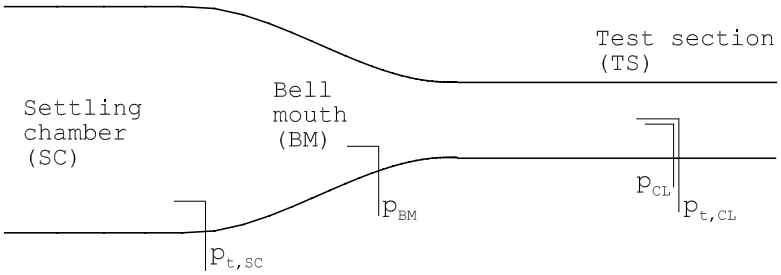

Figure 2. Schematic of tunnel survey locations.

pressure, $p_{t,CL}$ (CL = centerline), and static pressure, p_{CL}, which are used to calculate an incompressible dynamic pressure, $q_{CL,incompressible}$, using Eq. 8.

$$q_{CL,incompressible} = p_{t,CL} - p_{CL} \tag{8}$$

The difference between the settling chamber total pressure and the bell mouth static pressure, $q_{BM,incompressible}$, divided by the incompressible dynamic pressure from the centerline probe, $q_{CL,incompressible}$, as in Eq. 9, is the value of $\mathcal{K}$ for that set of pressure measurements.

$$\mathcal{K} = \frac{q_{BM,incompressible}}{q_{CL,incompressible}} \tag{9}$$

During operation of the tunnel, assuming that the upstream measurements of total and static pressures are sufficiently unperturbed by the presence of a model in the test section, the test section dynamic pressure, q_{TS}, static pressure, p_{TS}, and Mach number, M_{TS}, can be calculated as listed in Eqs. 10 through 12.

$$q_{TS,incompressible} = \mathcal{K} q_{BM,incompressible} \tag{10}$$

$$p_{TS,incompressible} = p_{t,SC} - q_{TS,incompressible} \tag{11}$$

$$M_{TS} = \sqrt{\frac{2}{\gamma - 1}\left[\left(\frac{p_{t,SC}}{p_{TS,incompressible}}\right)^{\frac{\gamma-1}{\gamma}} - 1\right]} \tag{12}$$

To account for compressibility effects, the test section dynamic pressure is subsequently updated using Eq. 13.

$$q_{TS,compressible} = \frac{1}{2}\gamma p_{TS,incompressible} M_{TS}^2 \tag{13}$$

If the static pressure survey point is moved downstream from the bell mouth to the test section, such that $p_{BM} = p_{TS}$, then Eq. 12 can be written as

$$M_{TS} = \sqrt{\frac{2}{\gamma - 1}\left[\left(\frac{p_{t,SC}}{p_{TS}}\right)^{\frac{\gamma-1}{\gamma}} - 1\right]} \tag{14}$$

B. Compressible Bernoulli Method

The incompressible methodology just discussed can be recast using the calorically perfect, compressible form of Bernoulli's equation. Equations 7 and 8 are replaced by Eqs. 15 and 16, respectively, to calculate the tunnel dynamic

pressure, q_{BM}, and the dynamic pressure from the centerline calibration probe, q_{CL}.

$$q_{BM,compressible} = \frac{\gamma}{\gamma-1} p_{BM}\left[\left(\frac{p_{BM}}{p_{t,SC}}\right)^{-\frac{\gamma-1}{\gamma}} - 1\right] \tag{15}$$

$$q_{CL,compressible} = \frac{\gamma}{\gamma-1} p_{CL}\left[\left(\frac{p_{CL}}{p_{t,CL}}\right)^{-\frac{\gamma-1}{\gamma}} - 1\right] \tag{16}$$

The equations for the calibration constant, $\mathcal{K}$, have the same form as shown in the previous section.

$$\mathcal{K} = \frac{q_{BM,compressible}}{q_{CL,compressible}} \tag{17}$$

After the calibration has been completed, the test section Mach number is calculated using Eq. 18.

$$q_{TS} = \mathcal{K}\, q_{BM,compressible} \tag{18}$$

There is no closed form solution for the static pressure with the compressible form of Bernoulli's equation, so Newton's method is used to solve Eq. 19 for p_{TS}.

$$q_{TS} = \frac{\gamma}{\gamma-1} p_{TS}\left[\left(\frac{p_{TS}}{p_{t,SC}}\right)^{-\frac{\gamma-1}{\gamma}} - 1\right] \tag{19}$$

The Mach number is calculated using the isentropic pressure relation written in Eq. 20.

$$M_{TS} = \sqrt{\frac{2}{\gamma-1}\left[\left(\frac{p_{t,SC}}{p_{TS}}\right)^{\frac{\gamma-1}{\gamma}} - 1\right]} \tag{20}$$

In the case of an empty tunnel simulation (no test article present) or a tunnel with a slotted test section with a surrounding static plenum chamber, the survey point in the bell mouth can be moved up to the test section, i.e., $p_{BM} \rightarrow p_{TS}$. The calibration constant $\mathcal{K}$ will approach one, eliminating the need for a calibration equation, Eq. 18. The methodology is greatly simplified where now the dynamic pressure in the test section is directly calculated using Eq. 15 and the tunnel conditions can be written as Eqs. 21 and 22.

$$q_{TS} = \frac{\gamma}{\gamma-1} p_{TS}\left[\left(\frac{p_{TS}}{p_{t,SC}}\right)^{-\frac{\gamma-1}{\gamma}} - 1\right] \tag{21}$$

$$M_{TS} = \sqrt{\frac{2q_{TS}}{\gamma p_{TS}}}, \tag{22}$$

C. Enthalpy Method

Using the control volume shown in Fig. 3, the rate of change of energy is integrated from the settling chamber through to the test section. For a real gas, the thermodynamic relations of energy, entropy and enthalpy can be functions of density, pressure and temperature. Omitting gravity, small losses due to the boundary layer, and assuming zero heat transfer in the process, an enthalpy conservation equation can be written as shown in Eq. 23 is applicable regardless of the thermodynamic path taken between these two states within the tunnel system. Further details on the derivation of the control volume equations can be found in Chapter 2 of Ref. [5].

$$0 = \left(H + \frac{1}{2}V^2\right)\Big|_2 - \left(H + \frac{1}{2}V^2)\right)\Big|_1 = H_2 + \frac{1}{2}V_2^2 - H_{t,1} \tag{23}$$

An expression for the velocity in the test section can be written by solving Eq. 23 for the velocity at station 2, as shown in Eq. 24.

$$V_2 = \sqrt{2\left(H_{t,1} - H_2\right)}, \text{ where} \tag{24}$$

$$H_{t,1} = H\left(\rho_{t,1}, p_{t,1}, T_{t,1}\right) \text{ and } H_2 = H\left(\rho_2, p_2, T_2\right)$$

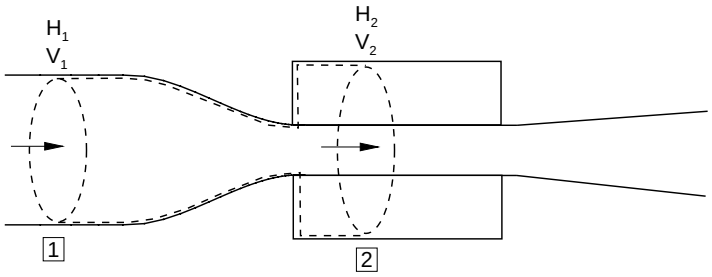

Figure 3. Schematic of a tunnel (including the surrounding static plenum chamber) control volume.

From the velocity, the dynamic pressure and Mach number can be written respectively in Eqs. 25 and 26.

$$q_{TS} = \frac{1}{2}\rho_2 V_2^2 \tag{25}$$

$$M_{TS} = V_2/c_2 \tag{26}$$

The calculation of $\rho_{t,1}$, T_2, c_2, and ΔH depend on the properties of the gas used for the simulations as detailed in Eqs. 27 through 31. Departure functions are used for calculation of the enthalpy, H, in the NTF controller software. Further information on the thermodynamic equations can be found in Hall [6] and Foster [7]. The same functionality is included in the back pressure controller and is used when thermally perfect gas simulations are performed.

$$\rho_{t,1} = \begin{cases} \text{Newton iteration to solve for } \rho_{t,1}, & \text{thermally imperfect gas} \\ \text{Parameter not required for ideal gas version} \end{cases} \tag{27}$$

$$T_2 = \begin{cases} \text{Newton iteration to solve for } T_2, & \text{thermally imperfect gas} \\ T_{t,1}\left(\frac{p_2}{p_{t,1}}\right)^{\frac{\gamma-1}{\gamma}}, & \text{ideal gas} \end{cases} \tag{28}$$

$$\rho_2 = \begin{cases} \text{Newton iteration to solve for } \rho_2, & \text{thermally imperfect gas} \\ \frac{p_2}{R_m T_2}, & \text{ideal gas} \end{cases} \tag{29}$$

$$c_2^2 = \begin{cases} \left(\frac{c_p}{c_v}\right)\left(\frac{\partial p}{\partial \rho}\right)_T, & \text{thermally imperfect gas} \\ \gamma R_s T_2, & \text{thermally perfect and ideal gas} \end{cases} \tag{30}$$

$$\Delta H = \begin{cases} H(\rho_{t,1}, p_{t,1}, T_{t,1}) - H(\rho_2, p_2, T_2), & \text{thermally imperfect gas} \\ c_p\left(T_{t,1} - T_2\right), & \text{ideal gas} \end{cases} \tag{31}$$

IV. Simple Tunnel Physical Description

A simple model "high-speed" leg tunnel was built to serve as a proof-of-concept test bed for the back pressure controllers discussed in Sec. C. Perspective and two-dimensional streamwise views of the tunnel are shown in Figs. 4 and 5, respectively. The tunnel flow medium enters a 4 meter diameter cylindrical test section coming from a 10:1 contraction ratio low speed settling chamber. The slotted-throat geometry had a 10 meter long test section surrounded by circular cross-section state plenum chamber approximately 8 meters in diameter. The test section and plenum chamber were connected via 8 equally spaced longitudinal slots spanning the full streamwise length of the plenum. A

closed throat tunnel geometry was constructed with the same internal contours as the slotted throat tunnel but with the slots and static plenum chamber removed. The 45 meter long diffuser downstream of the test section had a half-angle of approximately 2 degrees.

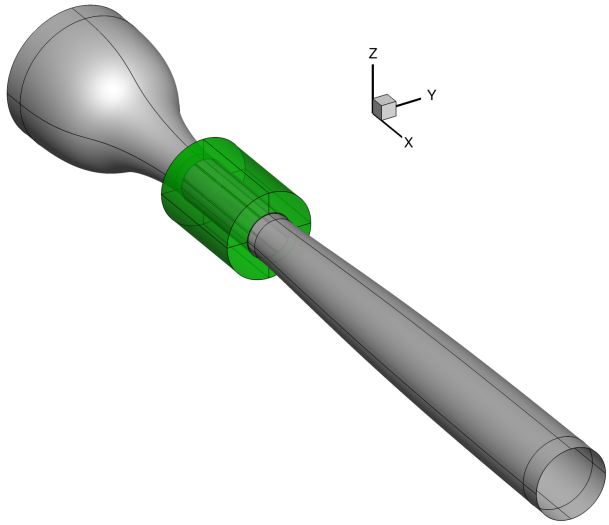

Figure 4. Perspective view of simple slotted throat wind tunnel with static plenum chamber.

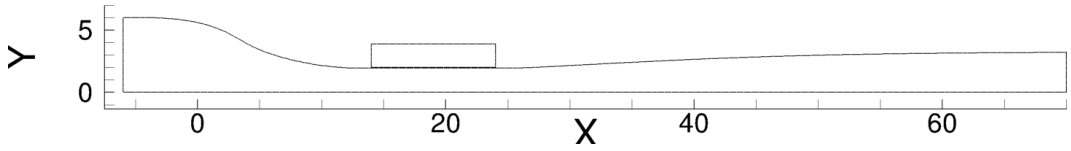

Figure 5. Stream-wise cross-section of simple slotted throat wind tunnel with static plenum chamber.

Flow survey points were located in the upstream low speed settling chamber at Sta. -5 (x = -5 m), inside the static plenum chamber for the slotted throat test section at Sta. 17 (x = 17 m), and test section centerline at Sta. 17 (x = 17 m) for the empty tunnel simulations. The static plenum survey point was moved to the test section wall for simulations using the closed throat configuration. The location of the flow survey points and schematic of the placement of the points are listed and shown in Table 1 and Fig. 6, respectively.

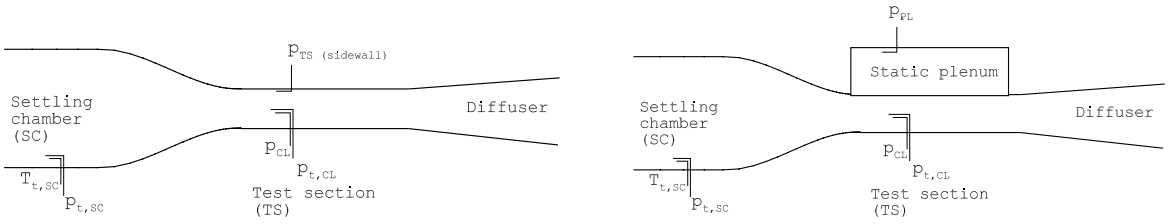

(a) Closed throat tunnel.

(b) Slotted throat tunnel.

Figure 6. Sketches of tunnel survey locations.

Table 1. Tunnel survey locations.

Location label		Streamwise	Lateral location	
Closed throat	Slotted throat	location (m)	Closed throat	Slotted throat
SC [1]	SC	-5.0	Center line	Center line
TS [2]	PL [3]	17.0	TS (sidewall)	Outer wall
TS	TS	17.0	Center line	Center line

[1] Low speed settling chamber.

[2] Test section.

[3] Static plenum chamber.

V. Computational Method

This section will present a brief overview of the computational method FUN3D, followed by a discussion of solution variable nondimensionalization procedure, boundary conditions used for wind tunnel simulations, and an example for setting pressure levels at the boundaries.

A. FUN3D

FUN3D is an unstructured three-dimensional, implicit, Navier-Stokes code. Solutions can be developed using either ideal gas assumptions (thermally and calorically perfect gas) or thermally perfect gas assumptions (thermally perfect and calorically imperfect gas). Roe's flux difference splitting [8] is used for the calculation of the inviscid terms. The Roe scheme was also used for the calculation of the Jacobian terms. Flux limiters were not used in any of the simulations. Ideal gas simulations can use the strong HANIM solver [9] when required to attain improved iterative convergence. Other details regarding FUN3D can be found in the manual [10], as well as in the extensive bibliography that is accessible at the FUN3D Web site `https://fun3d.larc.nasa.gov`.

B. Reference and freestream parameters

For simulations using the ideal gas path, the user input of Mach number, unit Reynolds number and temperature define the dimensional reference parameters: bulk viscosity, speed of sound, velocity, density, and pressure. The FUN3D solution variables are nondimensionalized by the reference temperature, reference density and the reference speed of sound as listed in Table 2. All of the reference parameters in the thermally perfect gas path are defined by the three user input parameters of velocity, density and temperature, in units of m/s, kg/m^3, and K, respectively, in the `fun3d.nml` namelist file. The thermally perfect gas path uses the reference velocity instead of the reference speed of sound to nondimensionalize velocity, pressure and energy, see Table 3.

The subscript 'ref' denotes a reference quantity, a tilde '˜' denotes a dimensional quantity, and the subscript '∞' denotes a freestream quantity. An exhaustive list of the variables used in the code are discussed in Sec. 2 of the FUN3D manual [10]. The nondimensional reference values for temperature, density and the speed of sound are 1.0 in the ideal gas path as listed in Table 3. Since pressure is nondimensionalized by $\tilde{\rho}_{\mathrm{ref}}\tilde{c}^2_{\mathrm{ref}}$ instead of $\tilde{p}_{\mathrm{ref}}$, the reference pressure for an ideal gas in FUN3D is equal to $1/\gamma$.

C. Boundary conditions

An internal flow simulation is fully defined when the total pressure, total temperature and velocity flow angle at the inflow boundary and static pressure at the outflow boundary are specified. The ideal gas path boundary conditions are normalized by the reference (for external aerodynamics the freestream) static pressure and temperature, as used in Stitt [11]. Boundary conditions in the thermally perfect gas path are in MKS units, i.e., Pa and K for pressure and temperature, respectively. Details on the implementation boundary conditions used by the ideal gas path in FUN3D can be found in Carlson [12].

Table 2. FUN3D dimensional reference parameters.

Parameter	Units	Ideal gas	Thermally perfect gas
Density	kg/m^3	$\tilde{\rho}_{ref} = Re_L \tilde{\mu}_{ref}/\tilde{V}_{ref}$ [1]	$\tilde{\rho}_{ref}$
Velocity	m/s	$\tilde{c}_{ref} = \sqrt{\gamma R_m \tilde{T}_{ref}}$	$\tilde{V}_{ref}$
Pressure	Pa	$\tilde{\rho}_{ref}\tilde{c}^2_{ref}$	$\tilde{\rho}_{ref}\tilde{V}^2_{ref}$
Temperature	K	$\tilde{T}_{ref}$	$\tilde{T}_{ref}$
Enthalpy	m^2/s^2	$\tilde{c}^2_{ref}$	$\tilde{V}^2_{ref}$

[1] $\tilde{\mu}_{ref} = \tilde{\mu}_0 \left(\frac{\tilde{T}_{ref}}{\tilde{T}_0}\right)^{3/2} \left(\frac{\tilde{T}_0+110.33}{\tilde{T}_{ref}+110.33}\right)$ (kg/m-sec),
$\tilde{V}_{ref} = M_{ref}\tilde{c}_{ref}$ (m/s).

Table 3. FUN3D nondimensional reference parameters.

Parameter	Ideal gas	Thermally perfect gas
ρ_{ref}	1	1
V_{ref}	M_{ref}	1
p_{ref}	$1/\gamma$ [1]	$\tilde{p}_{ref}/\tilde{\rho}_{ref}\tilde{V}^2_{ref}$
T_{ref}	1	$\tilde{T}_{ref}$
c_{ref}	1	$\sqrt{\gamma \tilde{p}_{ref}/\tilde{\rho}_{ref}}$

[1] $p_{ref} = \frac{\tilde{p}_{ref}}{\tilde{\rho}_{ref}\tilde{c}^2_{ref}} = \frac{\tilde{p}_{ref}}{\tilde{\rho}_{ref}\gamma\tilde{R}_m\tilde{T}_{ref}} = \frac{1}{\gamma}$

$$\text{PTBC} = \begin{cases} \tilde{p}_t \text{ (Pa)}, & \text{thermally perfect gas path} \\ \tilde{p}_t/\tilde{p}_{ref}, & \text{ideal gas path} \end{cases} \tag{32}$$

$$\text{TTBC} = \begin{cases} \tilde{T}_t \text{ (K)}, & \text{thermally perfect gas path} \\ \tilde{T}_t/\tilde{T}_{ref}, & \text{ideal gas path} \end{cases} \tag{33}$$

$$\text{PBC} = \begin{cases} \tilde{p} \text{ (Pa)}, & \text{thermally perfect gas path} \\ \tilde{p}/\tilde{p}_{ref}, & \text{ideal gas path} \end{cases} \tag{34}$$

External aerodynamic simulations typically use the reference conditions as the freestream conditions, where $M_\infty = M_{ref}$, $\tilde{p}_\infty = \tilde{p}_{ref}$, and $\tilde{T}_\infty = \tilde{T}_{ref}$. The simulation of a rotorcraft-in-hover is a common exception to this where the reference Mach number is associated with the rotor tip speed and the freestream Mach number is set to a different, usually smaller, value via the `vinf_ratio` parameter in the `&reference_physical_properties` namelist. The normalization of aerodynamic and pressure coefficients, Eqs. 35 and 36, respectively, use the reference Mach number and are not changed by the definition of freestream.

$$\vec{C}_{\text{Forces}} = \frac{2}{M^2_{ref}} \vec{F}_{\text{viscous+pressure}} \tag{35}$$

$$C_p = \frac{2}{\gamma M^2_{ref}} \left(\frac{p}{p_{ref}} - 1\right) \tag{36}$$

The concept of 'freestream' for the wind tunnel will be defined as the current state of the flow in the test section. The goal is to set the outflow static pressure so that the Mach number in the test section, i.e., the freestream, is equal to the reference Mach number. If the freestream Mach number does not match the reference Mach number, the freestream static pressure in the test section will differ from the reference static pressure. The most noticable consequence of a reference condition mismatch will be a shift in the pressure coefficients. The simulation is in the correct state when the conditions in the test section match the reference conditions of the problem.

The following sections describes a method for setting up the boundary conditions for wind tunnel simulation.

1. Setting the inflow boundary conditions

Consider the simulation of the flow through a simple contraction section followed by a constant area test section as pictured in Fig. 7. The Mach number, pressure, and temperature occurring in the test section of the wind tunnel are of particular interest and are primarily driven by the upstream inflow total conditions and the downstream outflow static pressure (back pressure) [1, 13]. Though the Mach number in the test section can be increased or decreased somewhat

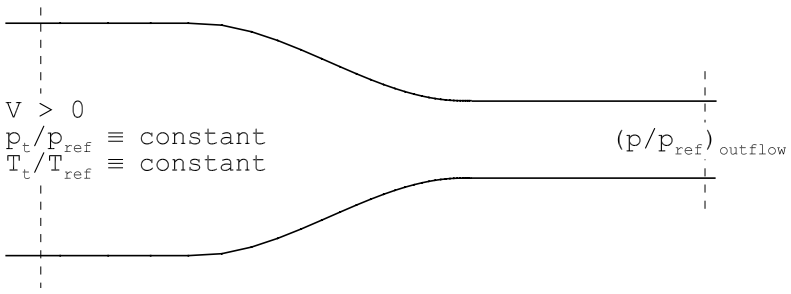

Figure 7. Sketch of simple converging duct.

arbitrarily as the static pressure imposed at the outflow boundary is decreased or increased, the proper value of the test section static pressure will only occur when the inflow boundary conditions, as defined in Eqs. 32 and 33, are set using the isentropic relation with the reference Mach number, that is, Eqs. 37 and 38.

$$\frac{\mathrm{p_t}}{\mathrm{p_{ref}}} = \frac{\tilde{\mathrm{p}}_\mathrm{t}}{\tilde{\mathrm{p}}_\mathrm{ref}} = \left(1 + \frac{\gamma - 1}{2}\,\mathrm{M}_\mathrm{ref}^2\right)^{(\gamma/\gamma-1)} \tag{37}$$

$$\frac{\mathrm{T_t}}{\mathrm{T_{ref}}} = \frac{\tilde{\mathrm{T}}_\mathrm{t}}{\tilde{\mathrm{T}}_\mathrm{ref}} = \left(1 + \frac{\gamma - 1}{2}\,\mathrm{M}_\mathrm{ref}^2\right) \tag{38}$$

When the Mach number measured in the test section is equal to the reference Mach number, the local static pressure will be equal the reference static pressure, i.e., $\mathrm{p} = \mathrm{p_{ref}} = 1/\gamma$. The pressure coefficient will then be zero, $\mathrm{C_p} = 0.$, at this condition, see Eq. 36.

2. Setting an initial outflow boundary condition

In the absence of previous knowledge and/or simulations with a particular tunnel configuration, a 'first guess' on the initial back pressure for a particular problem can be calculated using a mass flow conservation equation combined with the isentropic relations of Mach number, pressure, and temperature.

A Newton's method can be used to solve the transcendental equation, Eq. 39, to determine the Mach number at the outflow boundary (exit). The area ratio between the test section and the exit at the diffuser, $\mathrm{A_{TS}}/\mathrm{A_{exit}}$, will determine the static pressure at the outflow boundary.

$$\mathrm{M_{exit}}\left(1 + \frac{\gamma - 1}{2}\mathrm{M_{exit}^2}\right)^{\frac{1}{2} - \frac{\gamma}{\gamma-1}} = \mathrm{M_{TS}}\left(\frac{\mathrm{A_{TS}}}{\mathrm{A_{exit}}}\right)\left(1 + \frac{\gamma - 1}{2}\mathrm{M_{TS}^2}\right)^{\frac{1}{2} - \frac{\gamma}{\gamma-1}} \tag{39}$$

The pressure ratio at the tunnel test section and tunnel exit location are calculated using the relations listed in Eqs. 40 and 41, respectively.

$$\frac{p_{t,TS}}{p_{TS}} = \left(1 + \frac{\gamma - 1}{2} M_{TS}^2\right)^{(\gamma/\gamma-1)} \tag{40}$$

$$\frac{p_{t,exit}}{p_{exit}} = \left(1 + \frac{\gamma - 1}{2} M_{exit}^2\right)^{(\gamma/\gamma-1)} \tag{41}$$

In the absence of total pressure loss in the tunnel, i.e., $p_{t,exit} = p_{t,TS}$, the static pressure ratio is calculated using Eq. 42.

$$\frac{p_{exit}}{p_{TS}} = \frac{\left(p_{t,TS}/p_{TS}\right)}{\left(p_{t,exit}/p_{exit}\right)} \tag{42}$$

For the inviscid simulations, when the pressure, temperature and Mach number in the tunnel test section are equal to the reference conditions, then the exact boundary conditions are p_t/p_{ref} and T_t/T_{ref} for the inflow and p/p_{ref} for the outflow. These boundary conditions are expected to be very close to desired levels for viscous simulations. The PID-controller can then be engaged to drive the back pressure to the correct level.

VI. Results

In this section, simulations using the back pressure controller with empty closed- and slotted-throat test section configurations are discussed. For this proof-of-concept study, a single calibration point located along the centerline of the test section at Sta. 17 (x = 17m) is used for determining the Mach number in the test section. The veracity of this choice of a calibration survey geometry, i.e., a single point vs. a line or 2-D array of points, depends on the levels of pressure and temperature gradients throughout the test section, but should still serve the purpose of validating the controller methods.

As listed in Table 4, the numerical simulations were performed using the ideal and thermally perfect gas paths in the code. For the ideal gas solutions, called the 'compressible' gas path in FUN3D, the back pressure controller used ideal gas thermodynamic relations for determining the test section conditions. Simulations using the thermally perfect gas path, typically known as the 'generic' gas path in the code, used the back pressure controller based on the NTF control system software. Though no results will be shown in this report, an option is available to use a back pressure controller based on an equivalent, thermally perfect version of the NTF control system software. For the reference conditions used in this study, the difference between using thermally imperfect and thermally perfect equations for parameters such as the static temperature in the test section, Eq. 28, and Mach number, Eq. 26, were less than 0.005% and 0.05%, respectively. Additionaly, the TDT control equations have also been implemented in the controller software and included in the list for completeness, but no results are shown in this report.

Table 4. Survey of state equations.

Method	Thermal equation of state $p = f(\rho, T)$	Caloric equation of state
FUN3D - 'compressible'	$\rho R_m T$	$c_p \equiv$ constant [1]
FUN3D - 'generic'	$\rho R_m T$	$c_p = f(T)$ [2]
NTF control software	Beattie-Bridgeman [14]	$c_p = f(p, T)$ [3]
TDT control software	Redlich-Kwong [15]	$c_p = f(p, T)$ [3]

[1] Thermally and calorically perfect gas ≡ 'Ideal gas'.

[2] Thermally perfect and calorically imperfect gas ≡ 'Thermally perfect gas'.

[3] Thermally and calorically imperfect gas ≡ 'Thermally imperfect gas'.

Simulations using the ideal gas path in the code used a fixed ratio of specific heats, γ, equal to 1.4. The reference static pressure and temperatures were 86015.6 Pa and 280.0 K, respectively. Simulations using the thermally perfect

gas path were performed with a one temperature model of a 78% molecular Nitrogen (N_2) and 22% molecular Oxygen (O_2) mixture. The flow was assumed to be chemically frozen. The tunnel conditions for the simulations in this study are listed in Table 5.

Table 5. Tunnel inflow boundary condition and reference parameters.

Medium	Mach	Re (1/m)	$p_{t,SC}$	$T_{t,SC}$	T_{ref} (K)	ρ_{ref} (kg/m^3)	V_{ref} (m/s)
Perfect Air	0.500	1.02×10^7	1.186213[1]	1.0500[2]	280.0	1.0638	167.72
N_2O_2	0.499	9.99×10^6	101.42 kPa	294.0 K	280.0	1.0638	167.72

[1] Perfect air total pressure is normalized by the reference pressure, $\tilde{p}_{ref}$ = 85.5 kPa.

[2] Perfect air total temperature is normalized by the reference temperature, $\tilde{T}_{ref}$ = 280 K.

The following sections will compare solutions using the two gas paths and controllers on closed throat tunnel configuration to serve as a baseline, followed by a similar set of runs using the slotted throat tunnel.

A. Closed Throat Test Section.

In this section, a solution developed using the thermally perfect gas with the enthalpy-based back pressure controller (discussed in Sec. C), is compared to an ideal gas path solution using the controller documented in [1] with modifications as detailed in Sec. B. The two simulations used equivalent boundary and reference conditions as documented in Table 5 using the "N_2O_2" and "Perfect Air" flow media, respectively.

Solution residual and back pressure trends with respect to iteration for the ideal and thermally perfect gas solutions are plotted in Figs. 8 and 9, respectively. The continuity, energy and turbulent flow equations achieved close to machine zero solution residuals using a sequence of flow initialization, controller use, and fixing the back pressure for convergence. The two gas path solutions, comparing the solid black and dashed red lines in Fig. 10, produced nearly identical centerline Mach number distributions throughout the entire tunnel model. The solutions also achieved the requested Mach number with less than 0.1% error at the Sta. 17 calibration point. The Mach number distribution from the thermally perfect solution appears to be slightly above the ideal gas solution in the test section, see Fig. 10b, but still within 0.1% of the centerline distribution from the ideal gas solution. Similarly, the centerline pressure and temperature distributions in the test section for both gas path solutions, plotted in Fig. 11, are nearly identical and have the correct values at the calibration point.

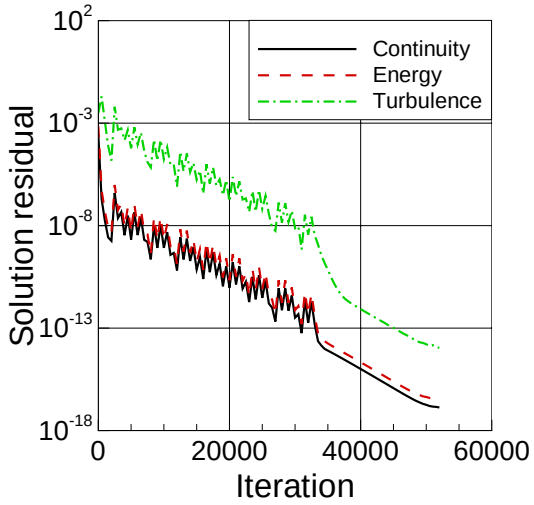

(a) Solution residual.

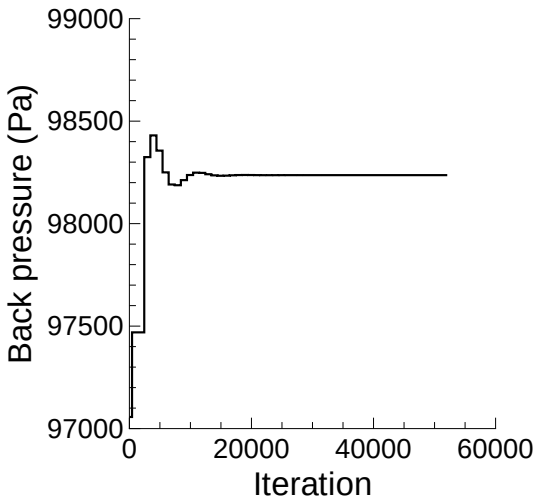

(b) Back pressure.

Figure 8. Solution history, closed throat, M = 0.5, compressible Bernoulli method controller, ideal gas.

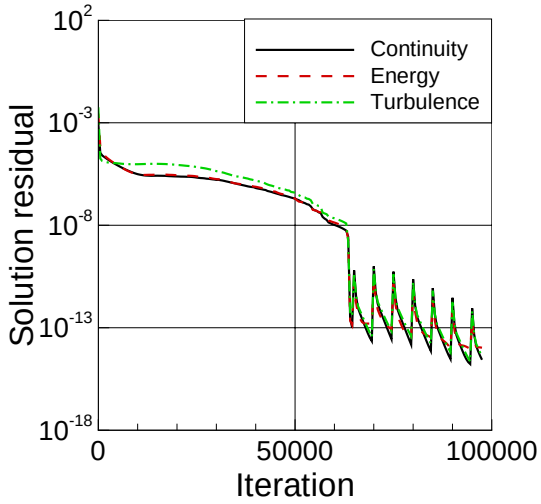

(a) Solution residual.

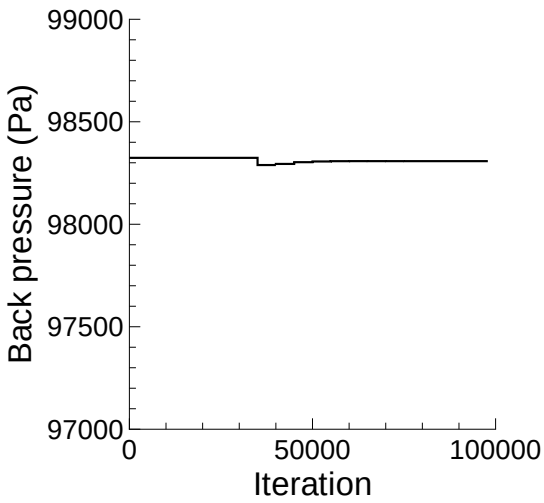

(b) Back pressure.

Figure 9. Solution trends, closed throat, M = 0.5, enthalpy method controller, thermally perfect gas.

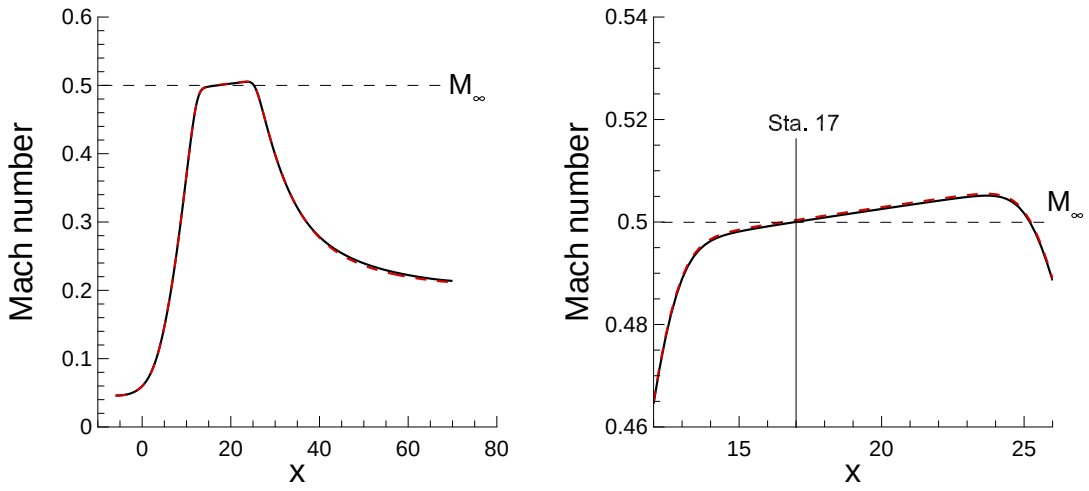

(a) High speed leg.

(b) Detail of test section.

Figure 10. Comparison of centerline Mach number distribution, closed throat, M = 0.5, ——, compressible Bernoulli method controller, ideal gas; – – – –, enthalpy method controller, thermally perfect gas.

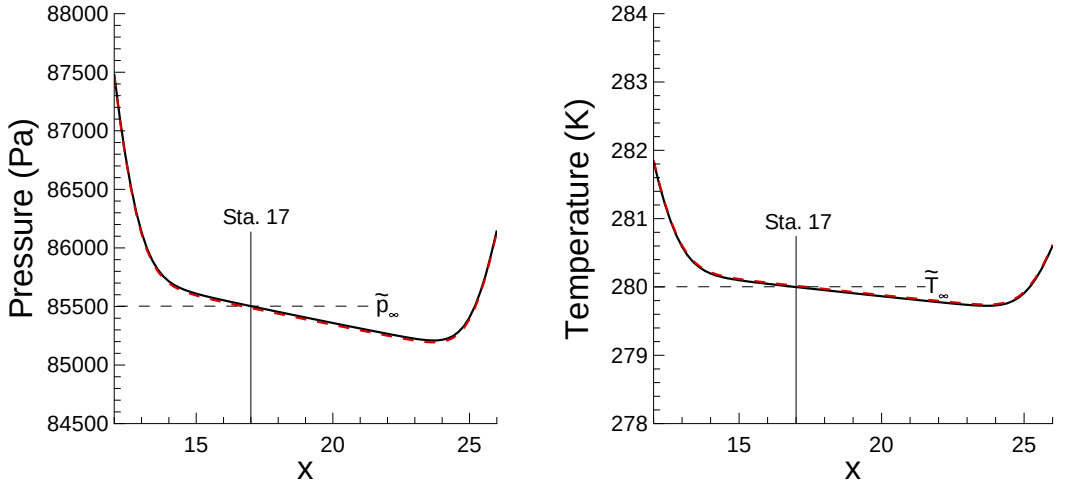

(a) Pressure.

(b) Temperature.

Figure 11. Comparison of centerline distributions, closed throat, M = 0.5, ——, compressible Bernoulli method controller, ideal gas; – – – –, enthalpy method controller, thermally perfect gas.

B. Slotted throat test section

Thermally perfect and ideal gas solutions developed using the slotted throat tunnel configuration described in Sec. IV, are discussed in this section. The tunnel reference conditions defining the simulations are the same and are listed in Table 5. The conditions for this proof-of-concept study were chosen to avoid conditions such as choked flow in the slots or test section. Iterative convergence to machine accuracy, in contrast to what was observed with the closed throat solutions discussed in Sec. A, was not achievable with either solution gas path, as seen in Figs. 12 and 13.

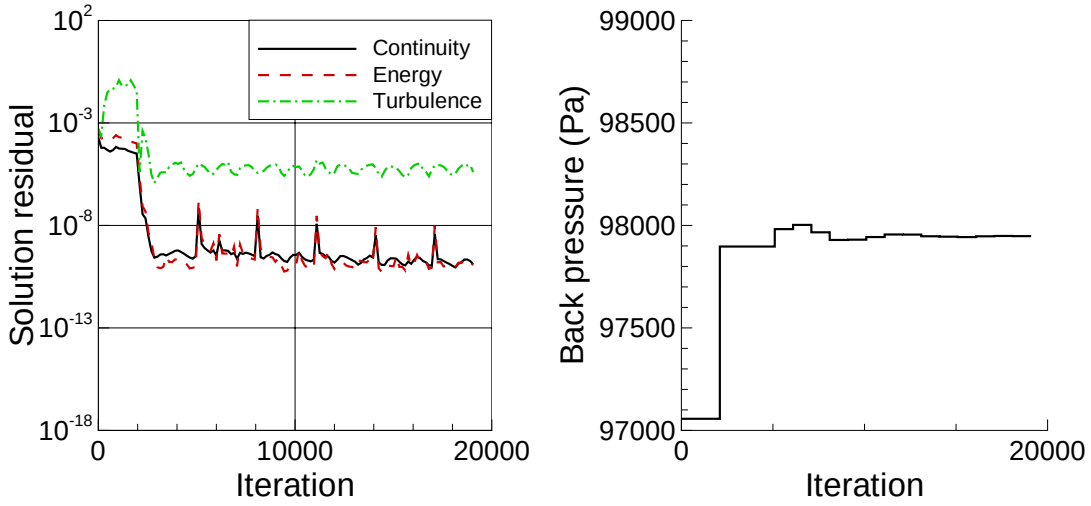

(a) Solution residual.

(b) Back pressure.

Figure 12. Solution history, slotted throat, M = 0.5, compressible Bernoulli method controller, ideal gas.

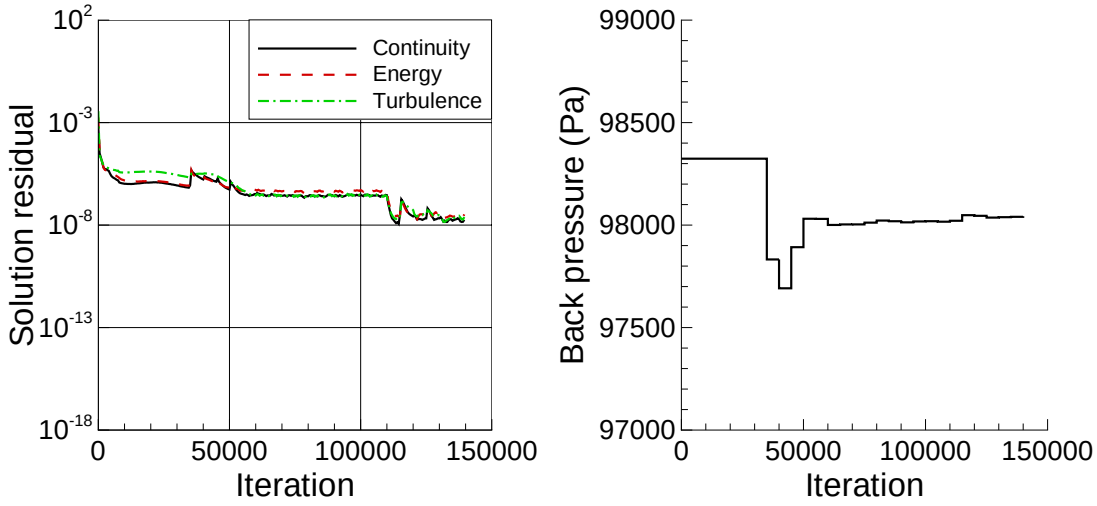

(a) Solution residual.

(b) Back pressure.

Figure 13. Solution history, slotted throat, M = 0.5, enthalpy method controller, thermally perfect gas.

The ideal gas path solution was run with first- and second-order iterations to eliminate the start-up transients before turning the back pressure controller on. The back pressure controller was activated for 10,000 iterations to converge to the requested test section Mach number, at which point the back pressure was frozen to allow the HANIM solver to work the solution residuals further down. The largely quiescent flow in the plenum chamber was a challenge

to properly resolve. The thermally perfect solution for the slotted throat tunnel simulation was equally difficult to iteratively converge as shown in Fig. 13. The thermally perfect solution was started using the boundary conditions from the ideal gas solution, so the back pressure adjustments from the controller were small by comparison with the ideal gas back pressure iterative trend.

Figures 14 and 15 compare the Mach number, pressure and temperature centerline distributions from the thermally perfect and ideal gas path solutions. The two gas path solutions using two different controller methods produce virtually identical centerline distributions and match the reference conditions at the calibration point. The Mach number, static pressure, and static temperature in the test section, from approximately 14m to 20m, are nearly constant in contrast to the significant streamwise gradients from the closed throat solution seen in Eqs. 10 and 11.

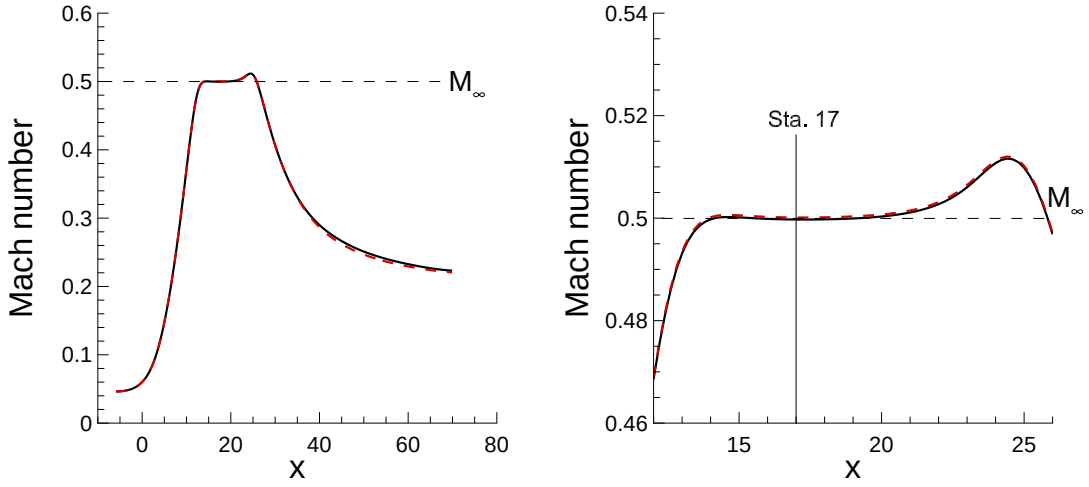

(a) High speed leg.

(b) Detail of test section.

Figure 14. Comparison of centerline Mach number distribution, slotted throat, M = 0.5, ——, compressible Bernoulli method controller, perfect air, ideal gas; – – – –, enthalpy method controller, N_2O_2, thermally perfect gas.

Contours of pressure and temperature at Sta. 17 for the ideal and thermally perfect gas path solutions are plotted in Figs. 16 and 17. Fairly uniform distributions of pressure are observed for both gas types and both solution gas types show a slightly higher pressure in the test section compared to the static plenum chamber. The static temperature contours were also very uniform in the test section for both solution gas types but the temperature in the static plenum was substantially higher in the thermally perfect gas solution comapred to the ideal gas solution.

Using the contour data presented in Figs. 16 and 17, the pressure and temperature are examined in more detail and are plotted along a radial line in Fig. 18. The two flow solution methods predicted a virtually identical and constant static pressure across the test section and static plenum, see Fig. 18(a).

In contrast, though the two flow solution methods (and the accompanying controller methodologies) predict the same static temperature in the test section, the results in the plenum chamber differed by approximately 3 K, or about 1% of the reference temperature. It is challenging to draw strong conclusions as to the root cause due to the scant amount of solution residual reduction. One possibility is the difference in the adiabatic wall boundary condition implementation between to two gas paths. When using the ideal gas path, the adiabatic wall temperature is set to the recovery temperature based on the flow Prandtl number, PR, and the reference Mach number, shown in Eq. 43. The thermally perfect (generic) gas path sets the adiabatic wall temperature to achieve zero energy flux through the wall.

$$\mathrm{T}_{\mathrm{adiabatic}} \;=\; 1 + \frac{\gamma - 1}{2}\sqrt{Pr}\mathrm{M}_{\mathrm{ref}}^2 \tag{43}$$

Measuring a static temperature directly from the CFD solution in the plenum that can be related to the static temperature in the test secton, as part of calculating tunnel conditions, could therefore be problematic. Using the isentropic relation in Eq. 28 to be representative of the static temperature of the test section is consistent with how the physical tunnel operates and was adopted for this study.

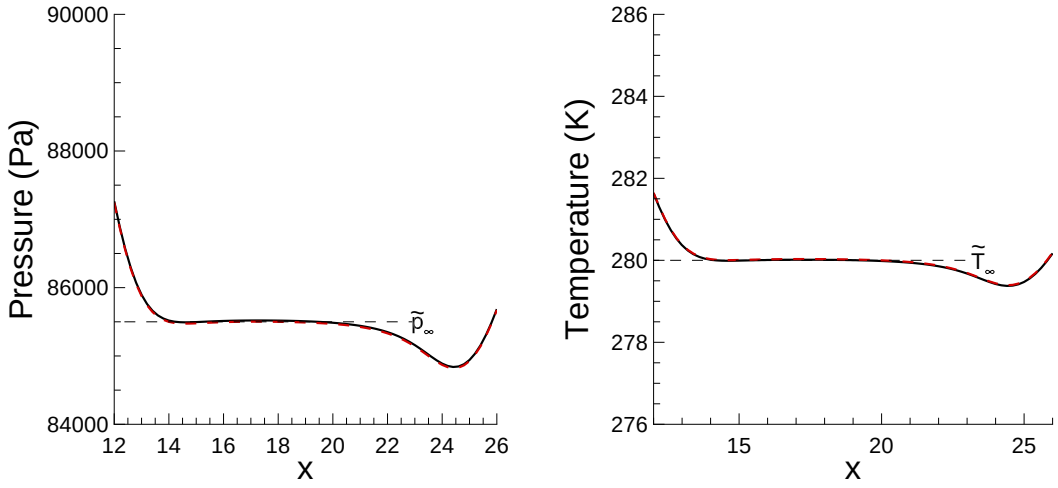

(a) Pressure.

(b) Temperature.

Figure 15. Comparison of centerline distributions, slotted throat, M = 0.5, ——, compressible Bernoulli method controller, ideal gas; – – – –, enthalpy method controller, thermally perfect gas.

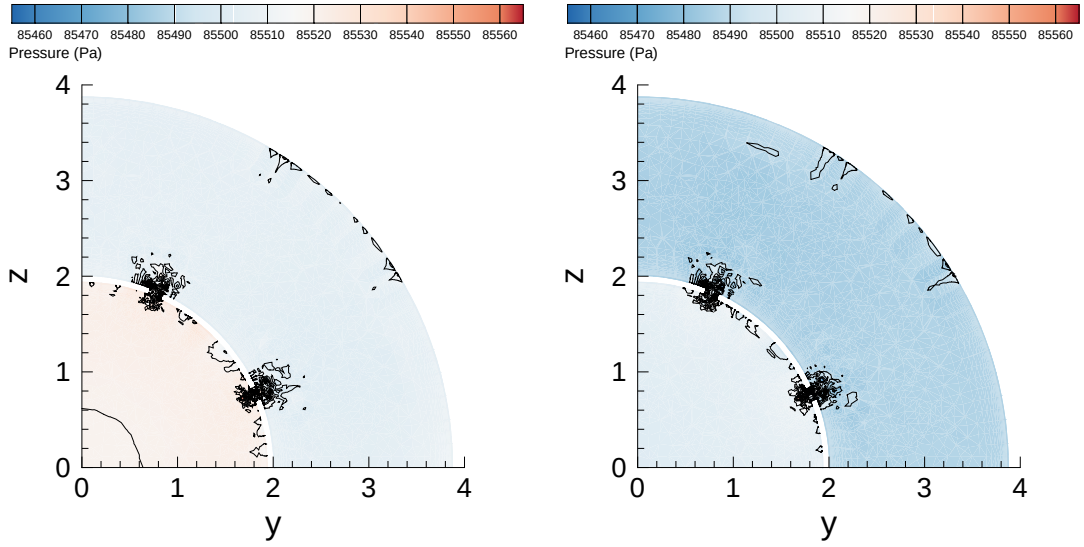

(a) Perfect air, ideal gas.

(b) N_2O_2, thermally perfect gas.

Figure 16. Comparison of test section pressure (Pascals) distributions, slotted throat, Sta. 17, M = 0.5.

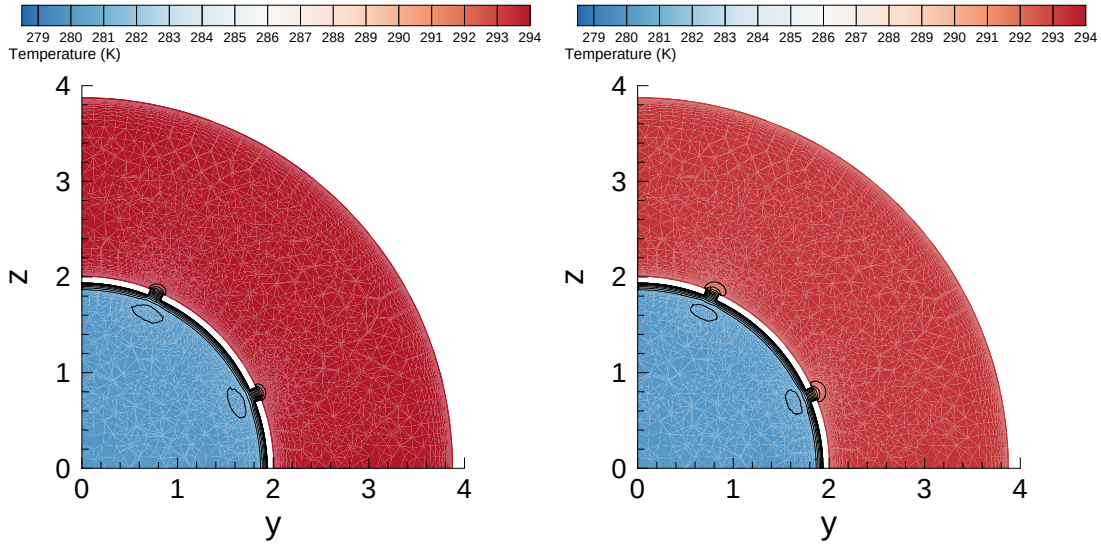

(a) Perfect air, ideal gas.

(b) N_2O_2, thermally perfect gas.

Figure 17. Comparison of test section temperature (Kelvin) distributions, slotted throat, Sta. 17, M = 0.5.

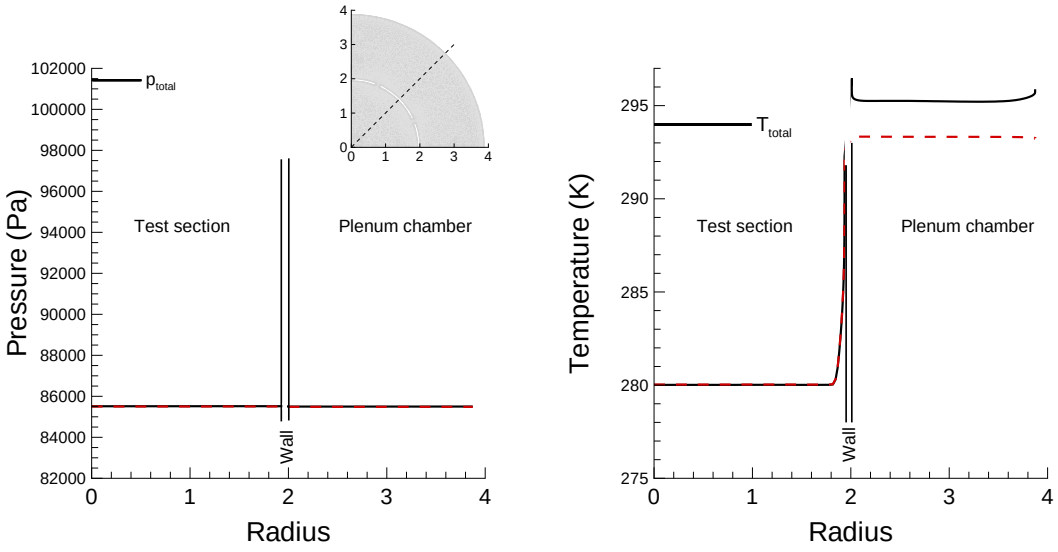

(a) Pressure.

(b) Temperature.

Figure 18. Comparison of radial profiles, Sta. 17, slotted throat, M = 0.5. ——, compressible Bernoulli method controller, perfect air, ideal gas; – – – – –, enthalpy method controller, N_2O_2, thermally perfect gas.

VII. Summary

A multispecies, thermally perfect, calorically imperfect gas back pressure controller method has been tested on closed and slotted throat test section tunnel geometries and compared with equivalent ideal gas results. A compressible Bernoulli equation controller method was used to drive the back pressure for the ideal gas simulations. An enthalpy equation based controller method was used for the thermally perfect, calorically imperfect generic gas simulations. No substantial difference in centerline Mach number, pressure or temperature distributions were observed between simulation gas thermodynamics for the closed throat tunnel. For the slotted throat tunnel simulation, while little difference was observed in the centerline distributions of Mach number, pressure, and temperature between the two simulation gas thermodynamic assumptions, there was a difference in the temperature flowfields in the static plenum chamber likely due to implementation differences in the adiabatic wall boundary condition. For tunnel conditions close to standard atmospheric conditions, the thermally perfect, calorically imperfect gas path solutions using an enthalpy-based back pressure controller matched closely with ideal gas path solutions using the compressible Bernoulli controller method.

References

[1] Carlson, J.-R., "Automated Boundary Conditions for Wind Tunnel Simulations," NASA TM–2018-219812, Mar. 2018.

[2] Rumsey, C. L. and Morrison, J. H., "Goals and Status of the NASA Juncture Flow Experiment," STO Applied Vehicle Technology (AVT) Panel, Progress and Challenges in Validation Testing for Computational Fluid Dynamics Paper Number AVT-246-03, Avila, Spain, Sept. 2016.

[3] Rumsey, C. L., Carlson, J.-R., Hannon, J. A., Jenkins, L. N., Bartram, S. M., Pulliam, T. H., and Lee, H. C., "Boundary Condition Study for the Juncture Flow Experiment in the NASA Langley 14x22-Foot Subsonic Wind Tunnel," AIAA Paper 2017-4126, June 2017.

[4] Pope, A. and Rae, W. H., *Low-Speed Wind Tunnel Testing*, New York : Wiley, 2nd ed., 1984, "A Wiley-Interscience publication.".

[5] Shapiro, A. H., *The Dynamics and Thermodynamics of Compressible Fluid Flow, Volume I*, "The Ronald Press Company, New York", 1953.

[6] Hall, R. M. and Adcock, J. B., "Simulation of Ideal-Gas Flow by Nitrogen and Other Selected Gases at Cryogenic Temperatures," NASA TP-1981-1901, Sep. 1981.

[7] Foster, J. and Adcock, J., "User's Guide for the National Transonic Facility Research Data System," NASA TM-1996-110242, Apr. 1996.

[8] Roe, P. L., "Approximate Riemann Solvers, Parameter Vectors, and Difference Schemes," *J. Comp. Phys.*, Vol. 43, 1981, pp. 357–372.

[9] Wang, L., Diskin, B., Nielsen, E. J., and Liu, Y., "Improvements in Iterative Convergence of FUN3D Solutions," AIAA Paper 2021-0857, 2021.

[10] Biedron, R. T., Carlson, J.-R., Derlaga, J. M., Gnoffo, P. A., Hammond, D., Jacobson, K. E., Jones, W., Kleb, W., Lee-Rausch, E., Nielsen, E., Park, M., Rumsey, C., Thomas, J. L., Thompson, K., Walden, A., Wang, L., and Wood, W., "FUN3D Manual: 13.7," NASA TM–2021-5010139, Nov. 2020.

[11] Stitt, L. E., "Exhaust Nozzle for Propulsion Systems With Emphasis on Supersonic Cruise Aircraft," NASA RP-1990-1235, May 1990.

[12] Carlson, J., "Inflow/Outflow Boundary Conditions with Application to FUN3D," NASA TM–2011-217181, October 2011.

[13] Jirasek, A., "Mass Flow Boundary Conditions for Subsonic Inflow and Outflow Boundary," *AIAA Journal*, Vol. 44, No. 5, 2006, pp. 939–947.

[14] Beattie, J. A. and Bridgeman, O. C., "A New Equation of State for Fluids. I. Application to Gaseous Ethyl Ether and Carbon Dioxide," *Journal of the American Chemical Society*, Vol. 49, 1927, pp. 1665–1667.

[15] Redlich, O. and Kwong, J. N. S., "On the Thermodynamics of Solutions. V. An Equation of State. Fugacities of Gaseous Solutions," *Chemical Reviews*, Vol. 44, No. 1, 1949, pp. 233–244.